sustainable chemistry

MDPI

Article

Trade-Offs Between Antioxidant Functionality and Physical Properties of Glycerol-Plasticized Chitosan Nanocomposite Films Containing Different-Sized Lignin Nanoparticles

Suteera Witayakran [1,2,3,†], Demi T. Djajadi [1,†], Helle J. Martens [1], Jens Risbo [4], Mogens L. Andersen [4] and Lisbeth G. Thygesen [1,*]

[1] Department of Geosciences and Natural Resource Management, University of Copenhagen, Rolighedsvej 23, DK-1958 Frederiksberg C, Denmark
[2] Polymer Chemistry, Saarland University, Campus C4 2, 66123 Saarbrücken, Germany
[3] Max Planck Institute for Informatics, Saarland Informatics Campus, Building E1 4, 66123 Saarbrücken, Germany
[4] Department of Food Science, University of Copenhagen, Rolighedsvej 26, DK-1958 Frederiksberg C, Denmark; mola@food.ku.dk (M.L.A.)
* Correspondence: lgt@ign.ku.dk; Tel.: +45-35331733
† These authors contributed equally to this work.

Abstract

This study investigated the effects of adding lignin nanoparticles (LNPs) to glycerol-plasticized chitosan nanocomposite films (pCS-LNP). Specifically, different LNP sizes (mean hydrodynamic diameters of about 70, 125 or 170 nm) and loadings (1, 3 or 5% of CS) were studied. The two largest LNP types aggregated mostly in the upper side of the cast films, while the smallest LNP type was found more uniformly throughout the film cross-section. The results showed a trade-off between film properties. Both UV barrier, visible light opacity and antioxidant properties increased with increasing LNP loading, while smaller LNPs resulted in higher stiffness and tensile strength than larger types. The radical scavenging activity of the films correlated with the migration of lignin-derived substances out of the films.

Keywords: lignin nanoparticle; chitosan; nanoparticle size; nanocomposite; antioxidant; UV barrier; functional food packaging

Academic Editor: Matthew Jones

Received: 18 December 2025
Revised: 17 February 2026
Accepted: 4 March 2026
Published: 11 March 2026

1. Introduction

Bio-based packaging materials, such as chitosan (CS), offer sustainable alternatives to petroleum-based plastics due to their renewability and biodegradability. CS is a linear polysaccharide of β-(1,4)-linked *N*-acetyl-D-glucosamine units derived from chitin [1]. It has excellent properties as a packaging material, including antimicrobial activity, non-toxicity, biocompatibility, biodegradability, film-forming properties, and decent mechanical strength [2,3]. However, to overcome the brittleness of pure CS films, glycerol is typically incorporated as a plasticizer to disrupt hydrogen bonding and increase chain mobility [4–8]. To further enhance functional properties, e.g., UV barrier function, antimicrobial activity, antioxidant activity, moisture or oxygen barrier properties, thermal stability, or mechanical strength, other additives/fillers can also be added. Various inorganic nanomaterials have been used as fillers in chitosan film, e.g., silver [9], zinc oxide [10,11], titanium oxide [12], carbon nanotubes [13], and nanoclay [14–17]. However, such additives are not entirely biodegradable, and some are potentially toxic. Consequently, the use of biodegradable

additives such as chitin nanowhiskers, cellulose nanocrystals, and lignin nanoparticles (LNPs), has been investigated [2].

Recently, LNPs have shown potential as bio-based additives to enhance the antioxidant, antimicrobial, UV barrier, and mechanical and thermal properties of packaging materials [18,19]. LNPs can be obtained through various chemical, physical, and biological methods using different types of fractionated or purified lignin, a by-product of pulping and biorefining processes [20,21]. These methods yield LNPs with varying shapes, sizes and stability. In packaging applications, LNPs or modified LNPs have been tested as nanofillers in several polymer matrices, e.g., polyvinyl alcohol (PVA) [21–23], (poly) lactic acid (PLA) [24,25], (poly) butylene adipate-*co*-terephthalate (PBAT) [26], and CS [22,27–29]. It is well understood that nanoparticle size significantly affects composite performance. Smaller particles offer a higher surface-area-to-volume ratio, enhancing interfacial bonding with the polymer matrix and increasing mechanical strength. However, the extent of improvement in mechanical properties also depends on various factors, including the type of matrix, nanoparticle size, dispersion quality, interface adhesion between particles and the matrix, and particle loading [30–32]. While several studies have incorporated LNPs into CS or CS-PVA films to improve UV barrier, antioxidant, and antibacterial properties, the specific influence of LNP size distribution remains under-explored, as most research utilizes fixed-size distributions [22,27–29].

Antioxidant activity is a key feature of functional packaging films, as it can help preserve food quality and nutrients, extending shelf life and reducing food waste. Research on antioxidant-containing functional packaging systems is steadily growing [33,34]. LNPs demonstrate strong antioxidant properties and have been evaluated as potential antioxidants in various applications [20]. LNPs have a high amount of phenolic hydroxyl groups, which enhance antioxidant activity via hydrogen atom transfer (HAT) and single electron transfer (SET) mechanisms [35]. Although the exact mechanism within CS films is not well understood, earlier research on lignin-incorporated biopolymers indicates that antioxidant efficiency is largely governed by the migration of phenolic compounds from the polymer matrix into the food contact surface [22,36]. This migration is typically a diffusion-controlled process, regulated by matrix swelling and the interfacial affinity between the filler and polymer chains. Additionally, Crouvisier-Urion et al. proposed a surface activity mechanism, where radical scavenging mainly takes place at the film interface rather than through deep migration [37]. However, the specific interplay between LNP particle size, loading density, and their migration kinetics in CS films, as well as whether such optimizations that affect the film's structural integrity, still needs thorough investigation. Specifically, it is important to identify which parameters influence LNP antioxidant functionality and whether improved antioxidant properties might compromise other film qualities.

In this study, we examined a fully bio-based film made from glycerol-plasticized CS films enhanced by the addition of LNPs. We specifically explored how three different sizes of LNPs, added at various loadings, influence the film's properties. The mechanical, physical, optical, and chemical properties of the films were characterized and compared to antioxidant activity. The radical scavenging activity (RSA) of the films was measured using both a spectrophotometric assay and electron spin resonance (ESR) spectroscopy to identify key parameters for antioxidant release from CS films. Understanding how LNPs improve CS film properties and provide antioxidant properties will help the continued efforts to develop functional, bio-based food packaging materials.

2. Materials and Methods

2.1. Material

High molecular weight CS (degree of deacetylation 76%, viscosity of 1218 cP) was purchased from Sigma-Aldrich (St. Louis, MO, USA). Soda lignin Protobind 1000 (TaNovis AG, Rüschlikon, Switzerland) was used as the starting material to prepare colloidal LNPs. All chemicals, glacial acetic acid and acetone (Merck KGaA, Darmstadt, Germany), glycerol (VWR International bvba, Leuven, Belgium), 2,2-diphenyl-1-picrylhydrazyl (DPPH) (95%) (Thermo Fisher Scientific Inc., Waltham, MA, USA), and ethanol (96%) (VWR International S.A.S, Briare, France), were purchased and used as received.

2.2. Preparation and Characterization of LNPs

LNPs were prepared from Protobind 1000 using three slightly different protocols to produce particles with different sizes based on modifications of previous studies [38,39]. Soda lignin was solubilized in an acetone–water mixture 3:1 (v/v) after stirring at room temperature (3 h at 22 °C) to create 0.5–1% (w/v) suspensions. The suspensions were vacuum-filtered using a glass microfiber filter GF/D (Whatman International Ltd., Maidstone, UK) and rapidly poured into deionized water under vigorous stirring, giving a three or five times mass-based dilution depending on the masses of the solvents used. The solvent was removed using a rotary evaporator at 40 °C, Rotavapor R-300 (BÜCHI Labortechnik GmbH, Essen, Germany) to obtain a concentration of at least 0.2% dry matter. The different methods for the preparation of the LNPs were as follow: LNP1 was created in 0.5% (w/v) suspension and diluted five times (w/w), LNP2 was created in 1% (w/v) suspension and diluted five times (w/w), LNP3 was created in 1% (w/v) suspension and diluted three times.

The hydrodynamic diameter, polydispersity index (PDI), and zeta potential of the LNPs were measured using a Zetasizer Nano ZS (Malvern Panalytical Ltd., Malvern, UK) in five technical replicates. The morphology of the LNPs was examined by negative-contrast transmission electron microscopy (TEM) as follows. A drop (2 µL) of LNP solution was placed on a carbon film-coated, 400-mesh grid and incubated for 30 s. Liquid was wicked away from the grid using a wetted wedge of filter paper, then negative staining was performed by covering the grid with a drop of aqueous 2.5% uranyl acetate (filtered through a 0.02 µm syringe filter) for 2 min. After wicking away excess stains, the grids were air-dried and placed in a Philips/FEI CM 100 transmission electron microscope (Philips, Eindhoven, Netherlands) operated at 80 kV. Images were collected at a magnification of 25,000× and 92,000×. The experiment was repeated for three grids per LNP size, and at least 10 images were obtained from each grid. Empty grids were used as control for the technique. To determine a representative particle size distribution, a total of at least 200 particles were measured for each film. The measurements were performed within entire images, excluding particles touching the image border. The resulting data were used to estimate the mean particle size and standard deviation.

2.3. Preparation of Films

Three different types of films were prepared: glycerol-plasticized chitosan films enhanced by addition of LNPs (pCS-LNP films), glycerol-plasticized chitosan film without addition of LNPs (pCS film), and pure chitosan film (CS film); the latter two served as controls. All films were prepared by the solvent casting method. CS solution was prepared by adding 1.5% (w/w) of CS to 1.5% (v/v) acetic acid under magnetic stirring at 70 °C for 4 h. Then, the solution was continuously stirred at room temperature overnight. The obtained viscous CS solution was centrifuged at 3500× g for 10 min to remove any undissolved CS particles. Then, the proper amount of CS solution was mixed with the prepared LNP

suspension at different loadings (0, 1, 3, and 5% (*w*/*w*) based on CS mass) to obtain the film at a total of 1% (*w*/*w*) of CS+LNP mass. 25% (*w*/*w*) glycerol with respect to CS+LNP mass was added into the solution as a plasticizer, and the mixture was then stirred at 600 rpm for 30 min. The film-casting solution was allowed to stand for 1 h to remove air bubbles. Then, 95 g of the solution was poured into an acrylic mold (150 × 150 mm) and dried at room temperature for four days. Subsequently, the films were peeled from the acrylic mold and stored in a desiccator at room temperature for at least 48 h before testing. The thickness of the films produced was approximately 50 µm (Table S1).

The pCS-LNP films are labeled based on the following format: pCS-LNP type-LNP loading. For example, the film prepared by adding 1% (*w*/*w*) of LNP1 is named pCS-LNP1-1. The CS and pCS films were prepared similarly but without glycerol and LNPs for CS, and without LNPs for pCS. Table 1 gives an overview of film names used throughout the article.

Table 1. Overview of film names used throughout the article.

Film Name	LNP Type (Size)	LNP Concentration (%*w*/*w*)
CS	Chitosan, no LNPs added	0
pCS	Glycerol-plasticized chitosan, no LNPs added	0
pCS-LNP1-1 pCS-LNP1-3 pCS-LNP1-5	LNP1: 0.5% (*w*/*v*) suspension, diluted five times (*w*/*w*)	1 3 5
pCS-LNP2-1 pCS-LNP2-3 pCS-LNP2-5	LNP2: 1% (*w*/*v*) suspension, diluted five times (*w*/*w*)	1 3 5
pCS-LNP3-1 pCS-LNP3-3 pCS-LNP3-5	LNP3: 1% (*w*/*v*) suspension, diluted three times	1 3 5

2.4. Characterization of pCS-LNP Films

2.4.1. Determination of Moisture Content, Water Solubility, and Swelling Degree

The films were cut into 20 × 20 mm pieces. The initial air-dried weight was denoted as W. The films were then dried at 105 °C in an oven until constant weight was reached (denoted as W_0). Moisture content was determined using the following equation:

$$\text{Moisture content (\%)} = [(W - W_0)/W] \times 100. \quad (1)$$

For water solubility, the dried films were immersed in 20 mL deionized water in a glass beaker and then shaken in a shaker incubator at 150 rpm at 25 °C for 24 h. Then, the films were dried at 105 °C until constant weight was reached (denoted as W_t). The solubility percentage was calculated using the following equation:

$$\text{Water solubility (\%)} = [(W_0 - W_t)/W_0] \times 100. \quad (2)$$

To determine the degree of swelling, the dried films were immersed in deionized water for 24 h at 25 °C. The films were then taken from the water, and the surface water was removed using filter paper before weighing (W_s). The degree of swelling was calculated using the following equation:

$$\text{Swelling degree (\%)} = [(W_s - W_0)/W_0] \times 100. \quad (3)$$

All measurements were performed in triplicate for each sample.

2.4.2. Determination of Film Thickness

Film thickness was determined using a digimatic micrometer gauge, MDC-1" SFB (Mitutoyo Corporation, Kawasaki, Japan) with a reported accuracy of 0.001 mm. Reported values are averages of thicknesses from at least 10 random locations per sample.

2.4.3. Mechanical Properties

Tensile strength, Young's modulus of elasticity, and percent elongation at break for each film were determined with a universal testing machine, Autograph AGS-X (Shimadzu Corporation, Kyoto, Japan), equipped with a 100 N load cell. The films were cut into rectangular strips measuring 15 × 100 mm and conditioned in a desiccator at about 0% RH at 23 °C for at least 24 h before testing. The initial gauge length was 50 mm. The crosshead speed was set to 10 mm/min. Each type of film was tested with at least five replicates, and the average value was reported.

2.4.4. Opacity and Optical Properties

Film opacity and optical properties were measured using a UV spectrophotometer (Ocean Optics, Dunedin, FL, USA). The films were cut into 10 × 40 mm rectangular pieces and placed inside the test cell of the spectrophotometer. A blank cell was used as a reference. The film opacity was determined as reported previously [40]. This implies that the absorbance of the films was measured at 600 nm, and the opacity was calculated using the following equation: Opacity = A_{600}/d, where A_{600} is the absorbance of the film at 600 nm, and d is the film thickness in mm. The full range (200–800 nm) opacity curves obtained are included in the Supplementary Materials (Figure S1). Three different sections were scanned from each film.

2.4.5. Antioxidant Activity

DPPH Free Radical Scavenging Assay

Based on previous work [37], the radical scavenging activity (RSA) of the films was measured using the reaction with the free stable radical 2,2-diphenyl-1-picrylhydrazyl (DPPH), with modifications to make it suitable for microplate measurement. DPPH absorbs strongly at 517 nm, giving rise to a deep purple color. When DPPH is converted to a reduced form (DPPH-H) by accepting either a hydrogen atom or an electron from an antioxidant species (in this case a phenolic compound), the initial purple color is lost [40]. The reaction kinetics of pCS and all pCS-LNP films were followed by the reduction in absorbance of the DPPH at 517 nm for 5 h in a dark room. Briefly, the film (40 mg) was put into a 2 mL tube and immersed in 0.1 mM DPPH ethanol solution (2 mL). The tube was shaken in the thermomixer at 25 °C at 500 rpm. By submerging the whole film in an ethanol solution containing DPPH radical (instead of using alcohol extracts of the films as in the conventional DPPH assay [41]), it imitates the antioxidant mechanism of a film in direct contact with a food product. This test was possible because chitosan is insoluble in ethanol [37], and consequently, the film structure was intact for the 5 h duration of the test.

For measurement, 200 µL of the reaction solution was taken out at 0.5, 1, 2, 3, 4, and 5 h reaction time, and the absorbance at 517 nm was determined using a microplate reader SpectraMax® i3 (Molecular Devices LLC, San Jose, CA, USA). All measurements were performed in triplicate. For each time point, the radical scavenging activity based on DPPH was calculated using the following equation:

$$\text{RSA (\%)} = [(A_{DPPH} - A_{sample})/A_{DPPH}] \times 100, \quad (4)$$

where A_{sample} is the absorbance measured from the DPPH solution containing the film sample, and A_{DPPH} is the absorbance of the initial DPPH solution.

Quantification of Lignin-Derived Substances Migrating from Films into Ethanol

The pCS (LNP-free control) and pCS-LNP films with 5% (*w*/*w*) LNP loading were chosen for this study. The film (40 mg) was put into a 2 mL tube and immersed in 2 mL of ethanol solution. The tube was shaken in the thermomixer at 25 °C at 500 rpm. For measurement of migrating lignin-derived substances, 200 µL of the reaction solution was taken out at 0.5, 1, 2, 3, 4, and 5 h reaction time and the absorbance at 285 nm was determined using a microplate reader SpectraMax® i3 (Molecular Devices LLC, San Jose, CA, USA). The increase in migrating lignin-derived substances was expressed as $Abs_t - Abs_0$, where Abs_0 is the absorbance of the initial ethanol solution and Abs_t is the absorbance of the reaction solution at the time when the sample was taken. As chitosan is not soluble in ethanol [39] and the lignin was dissolved in acetone prior to LNP synthesis, the substances that migrated from the film during incubation in ethanol solution are likely lignin-derived phenolics, which was hence assumed in this study. The fact that no signal was seen for the control film strengthens this interpretation.

ESR Spectroscopy

ESR measurements of selected films were performed on a MiniScope MS-5000 ESR spectrometer (Freiberg Instruments GmbH, Freiberg, Germany). The films were cut into rectangular 3 × 40 mm strips, and the thickness and weight of each film sample were measured. The film sample was put in a 5 mm OD quartz tube for ESR measurement of the initial radical in the film with the following settings: magnetic field 332–342 mT, sweep time 60 s, modulation amplitude 0.5 mT, microwave power 10 mW, and room temperature with minimum lighting.

The free radical concentrations both in the original films and in the DPPH ethanol solution before and after reaction with the film were measured using ESR spectroscopy (Figure S2). For this part of the study, only the pCS-LNP films with the highest LNP content of 5% (*w*/*w*) and the DPPH time point at 30 min were selected. The films were transferred to a 2 mL tube, and 0.1 mM DPPH solution in ethanol was added in the ratio of 5 mg film to 250 µL DPPH solution. The reaction solution was subsequently diluted three times by adding ethanol. The reaction tube was then shaken in a thermomixer at 25 °C at 500 rpm for 30 min. The film was then removed, washed with ethanol, and allowed to dry. The solution was transferred to a 50 µL quartz capillary micropipette (BLAUBRAND intraMark, Brand GmbH, Wertheim, Germany), and the film was put in a quartz ESR tube (outer diameter: 5 mm). The dried film and the solution were measured with ESR using the aforementioned settings.

Radicals in the films and the solution were quantified by double integration of the first-derivative ESR signal. A weak pitch sample (Bruker, Billerica, MA, USA) containing a known number of unpaired spins (1.08×10^{13} spins/cm) was used as a reference for the films. The initial DPPH solution served as reference. The radical scavenging activity of the films was determined by the following equation:

$$RSA\ (\%) = [(H_0 - H_x)/H_0] \times 100, \quad (5)$$

where H_0 and H_x were the peak heights of the middle peak of the DPPH spectrum of the initial DPPH solution, and reaction solution, respectively.

2.4.6. Scanning Electron Microscopy (SEM)

To study surface morphology of the films, pieces of the prepared film, approximately 5 × 5 mm, were mounted onto metal stubs with double-sided tape, sputter-coated with gold in an EM ACE200 automated sputter coater (Leica, Wetzlar, Germany), and viewed with scanning electron microscopy (SEM) in a Quanta 200/FEI (Philips, Amsterdam, The Netherlands) at 10 kV, using 5000×, 30,000×, and 100,000× magnifications. The SEM images were taken from the film surface in contact with air during drying (the air side). The experiment was repeated in three randomly selected regions of the film.

2.4.7. Confocal Laser Scanning Microscopy (CLSM)

Pieces of the films, approximately 4 × 4 mm, were placed on diagnostic slides with the cast face upwards and covered with a coverslip (dry preparation). The films were imaged in a Leica (Leica Microsystems CMS GmbH, Mannheim-Oststadt, Germany) SP5x upright CLSM in xyz-mode using these settings: line average 2, zoom 6, objective 20xw, image dimensions 1024 pixels for width and height. Lignin autofluorescence was excited with an argon 514 nm laser at 25% power and emission was collected in 536–644 nm. The films were captured in their dry state to prevent swelling, which could lead to variations in thickness. It is also important to highlight that the laser did not result in the formation of craters or any other damage to the films. All z-stacks were approximately 60 µm in thickness and included approximately 70 sectioning steps, starting and ending the series a few µm above and below the film. At least five series were prepared for each sample. Confocal orthogonal views of the films were depicted using a SpectrumLog look-up table which highlights the LNPs. The image-series were imported into Fiji ImageJ freeware, version v 1.5 4r, (https://imagej.net/software/fiji/, URL accessed on 12 November 2025) as AVI files, and displayed in 3D in volume mode using the 3D viewer plug-in.

2.5. Statistical Analysis

The data were evaluated by analysis of variance (ANOVA) with post hoc analysis based on Duncan's test using IBM SPSS Statistics for Windows, version 28.0 (IBM Corp., Armonk, NY, USA). All tests were repeated at least three times. The results were expressed as mean ± standard deviation and considered statistically significant if $p < 0.05$.

3. Results

3.1. LNP Characterization

Sizes of the LNPs are shown in Table 2. The sizes of LNPs measured by both DLS and TEM showed a consistent trend: LNP1 < LNP2 < LNP3, i.e., they were not in conflict with each other. It is important to note that the particle sizes measured by TEM reflect the dehydrated form of the LNPs. These measurements are consistently smaller than the hydrodynamic diameters usually determined through dynamic light scattering (DLS), since TEM does not account for the solvent layer and surface hydration effects. The relatively high standard deviation observed in samples for TEM measurement indicates broad size distributions for all three LNP size classes in the dry state, assumingly due to agglomeration. Also, according to the TEM images (Figure 1a), the LNPs did not have a perfectly spherical shape, which further adds to the high within-type variation between the measured diameters. The zeta potential of the LNP dispersions (Table 2) indicated sufficient electrostatic repulsion to ensure colloidal stability of the LNPs in water [41]. To summarize, size and shape characterization results confirmed the successful production of LNPs with three different sizes, albeit with some overlap between size distributions, and with apparent agglomeration within the dry films.

Table 2. LNP sizes and dispersion.

LNP Type	Diameter (nm), TEM	Hydrodynamic Diameter (nm)	Zeta Potential (mV)	PDI
LNP1	56.54 ± 19.54	72 ± 1.15	−39.3 ± 1.81	0.224 ± 0.033
LNP2	78.05 ± 37.03	123 ± 0.65	−45.4 ± 0.65	0.11 ± 0.012
LNP3	136.06 ± 68.44	167 ± 1.21	−43.6 ± 1.33	0.078 ± 0.016

Values are expressed as mean ± standard deviation. PDI: polydispersity index measured by dynamic light scattering (DLS).

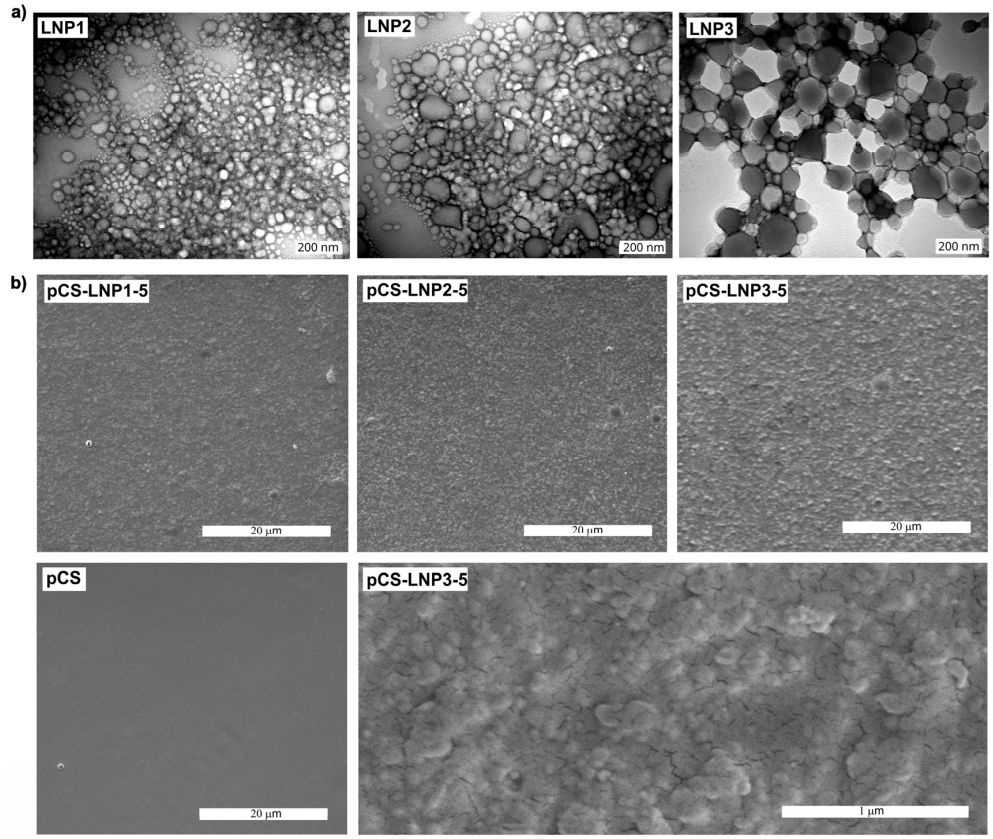

Figure 1. Microscopy of LNP and films. (**a**) negative contrast TEM images of LNPs. (**b**) SEM images of the air face of pure pCS and pCS-LNP films at 5% (w/w) LNP loading.

3.2. Physical and Mechanical Properties of Films

3.2.1. Characterization of LNP Distribution in Films

Glycerol-plasticized chitosan films containing LNPs were made by the solvent casting method. All nine types of pCS-LNP films had similar thicknesses, around 50 µm (Table S1). The pCS film without LNP had a smooth surface, whereas the addition of LNPs increased the surface roughness (Figure 1b). This surface roughness is visible on the upper surface, which was in contact with air, as opposed to the lower surface, which was in contact with the casting support as previously shown [37]. Films with the larger LNPs exhibited a higher tendency for particle aggregation at the same loading, resulting in increased surface roughness (Figure 1b), consistent with previous studies [27,28]. This can be attributed to the better dispersion of smaller particles in the pCS matrix during the solvent casting process, resulting in a uniform distribution of the smaller LNPs and a smoother film surface.

The rough air face and the smooth cast face can also be seen in CLSM (Figure 2). By employing a volume view of xyz image stacks following lignin autofluorescence excitation with a 514 nm argon laser, the distribution of lignin particles was visualized using a color scale. For all three films, a distinct granular layer with a high-intensity signal was observed along the air-facing surface of the film. This layer appeared denser in pCS-LNP1-5 than in

the others. Also interesting was the finding that the fluorescent signal in pCS-LNP1-5 was almost uniform and homogenous throughout the film matrix, whereas in pCS-LNP2-5, a multilayered structure was revealed in the upper half of the film, with stronger signal in the air side of the film. A layered structure was also observed for pCS-LNP3-5, but only close to the surface. Due to the inability to resolve individual LNP-sized particles in CLSM, the overall signal and visible structures likely arise from the aggregation of LNPs, as discussed by the authors of [40]. Aggregation was not limited to the surface but could be found throughout the films (Figure 2). Table 3 provides the ratio between the autofluorescent lignin signal close to the middle of the film relative to the maximum signal close to the air face. The mean values are based on three locations per film, and the lower ratio for pCS-LNP1-5 confirms the more uniform nature of the signal from this film, indicating a more uniform distribution of the smaller LNPs across the film.

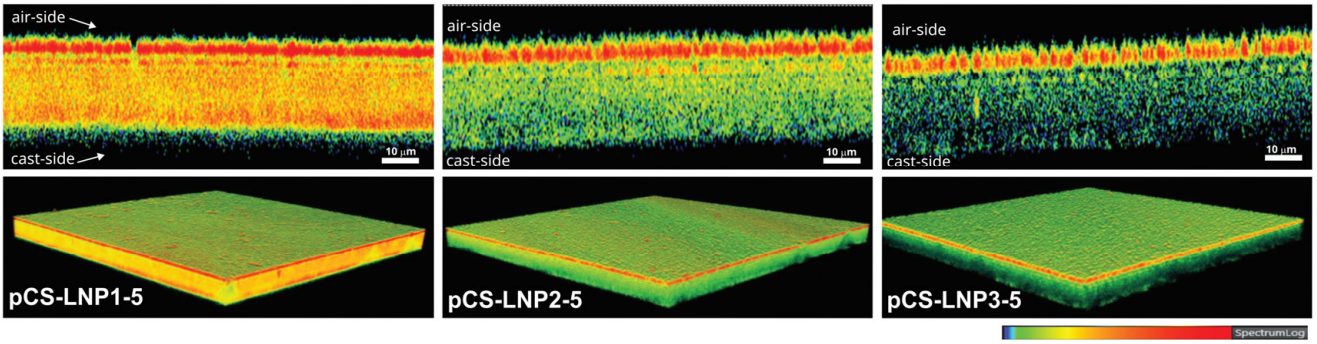

Figure 2. Confocal laser scanning microscopy images showing the distribution of lignin nanoparticles in pCS-LNP films with 5% (*w*/*w*) LNP loading. Top: orthogonal sections (optical xyz-stacks viewed from the side). Bottom: 3D representations of the image stacks. The color scale: red indicates a high-intensity signal of LNP.

Table 3. Quantification of CLSM signal. Signal from the center of the film relative to the maximum signal close to the air face.

Film	Signal Ratio
pCS-LNP1-5	0.18 ± 0.012
pCS-LNP2-5	0.34 ± 0.029
pCS-LNP3-5	0.41 ± 0.028

Values are expressed as mean ± standard deviation.

3.2.2. Moisture Relations

As expected, the pCS film had a relatively high moisture content (20.4%) in comparison to the pure CS film (3.6%) (Table 4) because glycerol is hydrophilic [7]. The addition of LNPs did not alter the moisture content of pCS-LNP films compared to pCS film. The water solubility of the pCS film (with 25% (*w*/*w*) glycerol) was 15.9% after soaking the film in water at 25 °C for 24 h. Although the result seems high, it is only half of the previous reports for pCS with 30% (*w*/*w*) glycerol, which was 27.4% [42]. The addition of LNPs did not affect the water solubility of the films significantly (Table 3).

The degree of water swelling was significantly reduced by adding LNPs to the films: the swelling of the pCS film was 30–70% higher than for the pCS-LNP films (Table 3). We suspect the lower swelling of pCS-LNP films compared to pCS film was caused by the hydrophobic nature of LNPs and by LNP–chitosan interaction. This interaction, likely between carboxyl and hydroxyl groups in the lignin phenolic backbone and the amine groups in the chitosan chain, could decrease the affinity of chitosan film to water [6,42,43]. A similar observation was made in other studies incorporating natural phenolic antioxidants

into biopolymers [42,43] and LNPs into pCS [28]. The reduction in water swelling of pCS-LNP has, in a previous study, been connected to a decrease in water vapor permeability and an increase in the contact angle with water [28], hence supporting the suggested mechanisms. However, in the present study, no trend is apparent among the LNPs with different sizes at various loadings (Table 4). Thus, further investigation is still needed to fully understand how LNP size and loading affect CS film moisture relations.

Table 4. Physical properties of pCS, pCS-LNP1, pCS-LNP2, and pCS-LNP3 films.

Sample	Moisture Content (%)	Water Solubility (%)	Swelling Degree (%)
pCS	$20.4 \pm 1.84^{b,c}$	15.9 ± 1.46^{d}	179.8 ± 0.12^{a}
pCS-LNP1-1	$20.3 \pm 1.12^{b,c}$	$17.1 \pm 0.54^{b,c,d}$	109.7 ± 1.55^{f}
pCS-LNP1-3	22.2 ± 1.87^{a}	16.2 ± 0.60^{d}	$128.6 \pm 5.32^{c,d}$
pCS-LNP1-5	$21.9 \pm 1.37^{a,b}$	$16.6 \pm 0.63^{c,d}$	144.1 ± 3.23^{b}
pCS-LNP2-1	$18.4 \pm 0.87^{d,e}$	$18.1 \pm 0.69^{a,b,c,d}$	147.1 ± 8.60^{b}
pCS-LNP2-3	17.2 ± 1.22^{e}	$19.2 \pm 0.34^{a,b}$	132.9 ± 7.58^{c}
pCS-LNP2-5	$19.4 \pm 1.06^{c,d}$	$18.8 \pm 2.69^{a,b,c}$	$126.6 \pm 2.83^{c,d}$
pCS-LNP3-1	$18.1 \pm 1.50^{d,e}$	19.5 ± 1.12^{a}	$120.7 \pm 6.55^{d,e}$
pCS-LNP3-3	17.5 ± 1.01^{e}	16.3 ± 0.80^{d}	$123.5 \pm 2.56^{c,d}$
pCS-LNP3-5	20.0 ± 1.31^{c}	$17.5 \pm 1.42^{a,b,c,d}$	$111.1 \pm 9.36^{e,f}$

Values are expressed as mean ± standard deviation. Different letters in the same column indicate significant differences ($p < 0.05$).

3.2.3. Mechanical Characterization

The mechanical properties, including Young's modulus, tensile strength, and elongation at break, are shown in Figure 3a–c. Typical stress–strain curves acquired from the tensile tests are exhibited in Figure 3d. Young's modulus, tensile strength, and elongation at break of the pCS film were 2350 ± 172 MPa, 100.5 ± 5.8 MPa, and 41.8 ± 6.6%, respectively. Elongation at break was relatively high, as expected from the literature [4]. When LNPs were incorporated into the pCS matrix at a loading of 1%, the stiffness of the film increased, although further effects were not seen for higher additions. Addition of the smallest particles (LNP1) resulted in a higher stiffness (Young's modulus) of the resulting films than for LNP2 and LNP3. However, LNP addition did not increase the tensile strength, and it was even reduced when adding bigger particles, i.e., LNP2 and LNP3. We speculate that the higher Young's modulus and tensile strength of the pCS film with LNP1 can be attributed to the uniform distribution of the smaller LNP particles, providing good interfacial contact between CS matrix and nanoparticles. The bigger LNP particles agglomerated more, which is known to induce adverse effects on the mechanical performances of polymer nanocomposites [30].

Figure 3c shows that LNP addition significantly decreased the elongation at break of the films. We speculate that this might be due to chemical interaction between chitosan and the phenolic groups of LNPs, which could reduce the free volume in the polymeric network, reducing the chain mobility and flexibility of pCS-LNP films [4]. None of the films exhibited a significant difference in elongation at break as a function of LNP size at the same LNP loading. These results are similar to a previous finding that adding LNPs significantly decreased the elongation at break while increasing the tensile strength [28]. The difference in tensile strength effect compared to [28] can be due to many factors, including the physicochemical properties of the chitosan (such as its Mw), the LNP particle size and concentration, and the type of plasticizer. In previous research [28], they utilized low-molecular-weight chitosan, smaller LNP particles (65 nm), and a eutectic solvent (DES) as a plasticizer, all of which differ from the current study. In the previous study, the control chitosan film had a tensile strength below 10 MPa, whereas in ours, it already reached 100 MPa (about ten times higher) even without LNPs. In contrast, adding LNPs in our current research did not significantly affect the tensile strength of chitosan films, only

producing a modest increase with the smallest (LNP1) particles. Although the addition of LNPs made the pCS film more brittle in the current study, the elongation at break is still higher than for non-plasticized CS film and comparable to other biopolymer films, which are typically more brittle than synthetic polymer films [44].

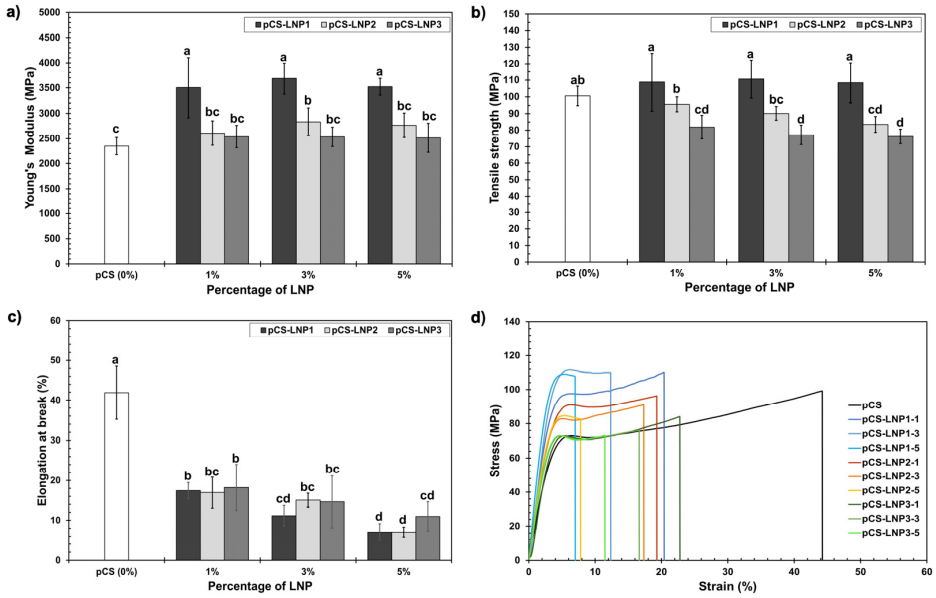

Figure 3. Mechanical properties of films. (**a**) Young's modulus, (**b**) tensile strength, (**c**) elongation at break, and (**d**) stress–strain curves of pCS, pCS-LNP1, pCS-LNP2, and pCS-LNP3 films at different LNP loading. Different letters above the error bars indicate significant differences ($p < 0.05$).

3.3. Opacity and UV Barrier Properties of Films

The ideal packaging film for light-sensitive products should have low opacity in the visible range, while at the same time blocking out UV radiation. Adding LNPs into pCS films significantly increased film opacity (Figure 4a). The pCS film (without LNPs) showed the lowest opacity (1.27 ± 0.09), similar to pCS-LNP1-1, while the opacity increased with increasing LNP loading for all LNP sizes. However, as shown in Figure 4a, even the most opaque films (containing 5% LNPs) still exhibited transparency. At the same LNP loading, the film with the smallest LNPs, pCS-LNP1, had significantly lower opacity than the films with larger particles, i.e., pCS-LNP2 and pCS-LNP3. This can presumably be attributed to the more uniform distribution of smaller LNP1 than LNP2 and LNP3 in the pCS film.

Since LNPs have shown excellent UV barrier property in many studies [24], a potential application for pCS-LNP films is as biodegradable UV-blocking films. The effect of LNP size and loading on the UV-blocking properties was investigated by measuring the UV-vis transmittance in the wavelength range of 200–800 nm, as shown in Figure 3b. The pCS film without LNP showed high transmittance across the entire UV region. At 1% (*w*/*w*) LNP, all pCS-LNP films showed good blocking performance in the UV region (200–400 nm), especially in the UV-C range (200–280 nm) where the transmittance was reduced to below 2%. Increasing the LNP loading improved the UV barrier performance without affecting the visible light transparency. This agrees with other studies involving nanocomposite films containing LNPs [21,23,27,28]. Our results show that by increasing LNP loading to 3% (*w*/*w*), all the UV-C (200–280 nm tested range), UV-B (280–320 nm), and some UV-A (320–350 nm) radiations were blocked (Figure 4b). When LNP loading increased to 5% (*w*/*w*), UV light transmittance was reduced to below 1%. This is comparable to the results of previous studies [22,27,28]. At the same LNP loading, all pCS-LNP films exhibited similar characteristics of the UV transmission spectrum, hence the LNP size had no effect on the UV barrier performance (Figure 4b). From Figure 4a, it is seen that the transmission

in the visible part of the spectrum is also affected (especially at low wavelengths), seen as an increased brown color (Figure 4a, right panel).

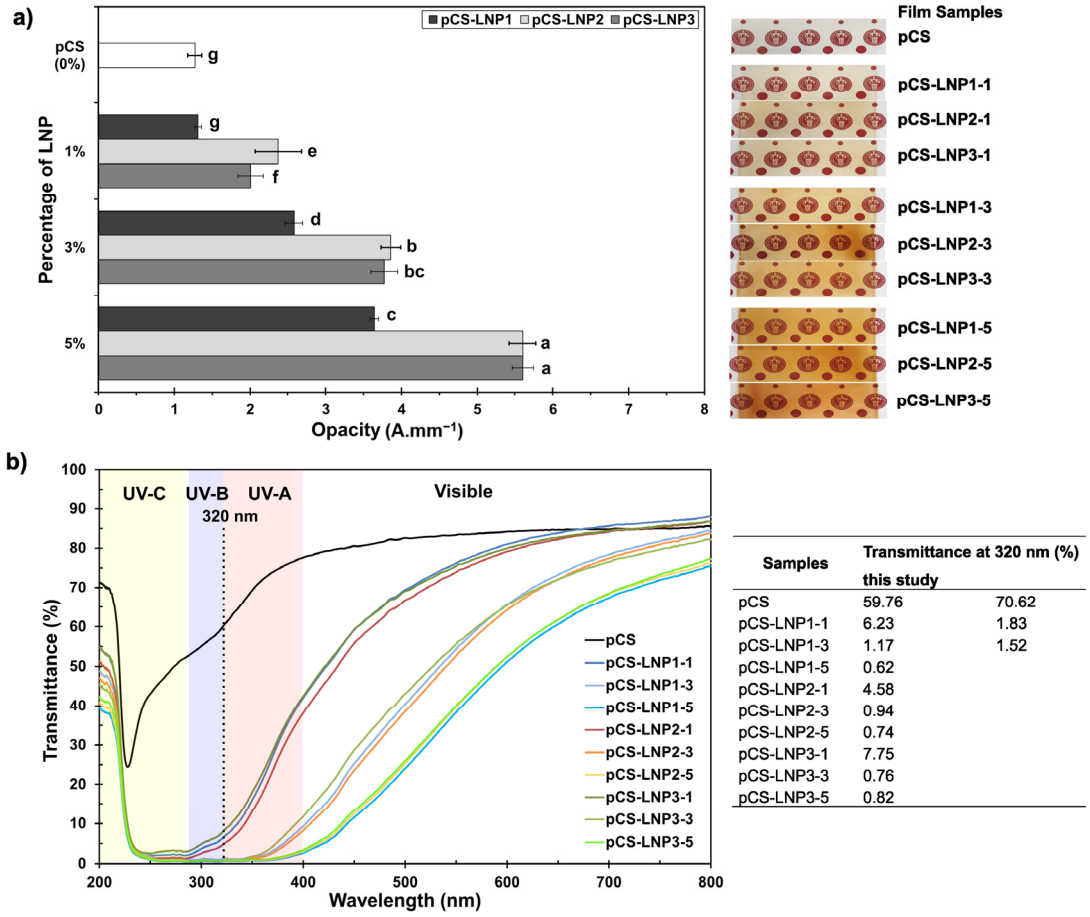

Samples	Transmittance at 320 nm (%) this study	
pCS	59.76	70.62
pCS-LNP1-1	6.23	1.83
pCS-LNP1-3	1.17	1.52
pCS-LNP1-5	0.62	
pCS-LNP2-1	4.58	
pCS-LNP2-3	0.94	
pCS-LNP2-5	0.74	
pCS-LNP3-1	7.75	
pCS-LNP3-3	0.76	
pCS-LNP3-5	0.82	

Figure 4. Optical properties of films. (**a**) Opacity (left) and physical appearance (right). (**b**) UV-vis spectra (left) and transmittance value at 320 nm (compared with data from [22]) (right) of pCS, pCS-LNP1, pCS-LNP2, and pCS-LNP3 films at different LNP loading. Different letters above the error bars indicate significant differences ($p < 0.05$).

3.4. Antioxidant Activity of the Films

3.4.1. Radical Scavenging Activity Assessed by the DPPH Assay

The ability of the LNP-containing films to scavenge radicals was clearly observed by the decolorization of DPPH ethanol solutions in contact with the films (Figure 5). The pCS film (without LNP) exhibited a small radical scavenging activity (RSA), which can be ascribed to the chitosan [45]. All pCS-LNP films showed significantly higher radical scavenging activities than the pCS film at all time points, and RSA increased with LNP loading, as reported in other studies [21–23]. After 30 min reaction time, all pCS-LNP films with 1% (*w*/*w*) LNPs provided similar low levels of RSA independent of LNP size, while RSA was higher at the higher LNP loadings (3 and 5%), where RSA also varied with LNP size. After 5 h, pCS-LNP2 films exhibited the highest RSA, followed by pCS-LNP3 and pCS-LNP1. The reaction rate of pCS-LNP1 slowed down after 30 min, resulting in lower final RSA than that of pCS-LNP2 and pCS-LNP3 (Figure 5a). In other words, although the pCS-LNP1 film (with the smallest and most well distributed particles) was expected to show the highest antioxidant activity of the pCS-LNP films due to a high surface area-to-volume ratio of the LNPs [20], the results of this assay showed the opposite.

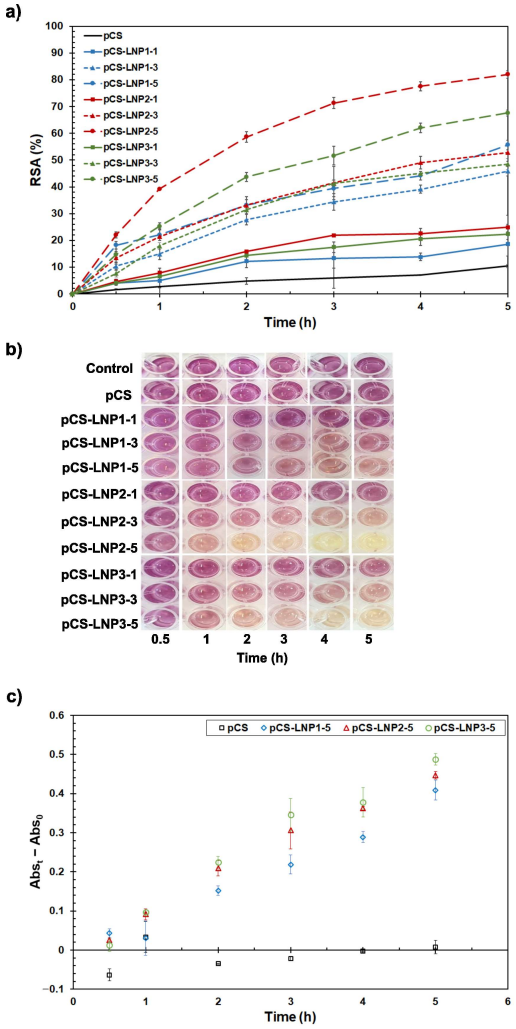

Figure 5. Antioxidant activity of films. (**a**) Radical Scavenging Activity (RSA) evaluated over time by the DPPH assay. (**b**) Corresponding color change in the DPPH ethanol solution over time during incubation with pCS and pCS-LNP films. (**c**) Absorbance at 285 nm due to migrating lignin-derived substances from the films when placed in ethanol pCS (LNP-free control) and (pCS-LNP films at 5% (*w*/*w*) of LNP). The pCS film shows negligible absorbance.

3.4.2. Released Lignin-Derived Substances

The release of lignin-derived substances from the three 5% films into ethanol over a 5 h period is shown in Figure 5c. Absorbance at 285 nm, indicative of phenolics, increased with time for all three films tested, with consistently higher absorbance for the largest LNPs, and lowest for the smallest. This suggests a slower diffusion rate of migrating lignin-derived substances from pCS-LNP1 than from pCS-LNP2 and pCS-LNP3. The dominant antioxidant effect of the films over time is therefore likely due to release of phenolic lignin-derived substances. The migration of these LNP fragments likely involve the interaction between the solvent and the films [46]. The slow release of these antioxidants from the pCS-LNP1 film was likely due to the uniform distribution of the small LNPs, which entrapped them better in the film matrix as shown by CLSM (Figure 2), and as indicated by the higher strength of this film than of those containing larger LNPs (Figure 3 and previous studies [27,28]). This mode of action also explains the result of the RSA assay reported in Section 3.4.1. As performed in this study, this assay seems to mostly quantify development over time in the RSA of released phenolics, and thus correlates with the rate of release of the lignin-derived substances.

3.4.3. Radical Scavenging Activity Assessed by ESR Spectroscopy

All pCS-LNP films gave a characteristic broad single-line ESR spectrum with no hyperfine structure, while the pCS gave no ESR signal (Figure 6a). The ESR signals in the pCS-LNP films likely arise from phenolic radicals of the LNPs that are long-lived due to immobilization in the films. These radicals may have been inherent in the native lignin, or generated during the lignin extraction process and the LNP synthesis [47]. The pCS-LNP2-5 film had the highest radical content (10.3×10^{15} spins/g), followed by pCS-LNP1-5 (8.3×10^{15} spins/g), and pCS-LNP3-5 (7.9×10^{15} spins/g) (Figure 6b). The RSA values calculated based on the loss of DPPH radicals in the solution after 30 min contact with the films correlate reasonably well with the original amount of radicals in the films (Figure 6b). They also agree with the spectrophotometric RSA assay results after 30 min where pCS-LNP2-5 gave the highest value while pCS-LNP1-5 and pCS-LNP3-5 were of similar value at ca. 10–20% (Figure 5a).

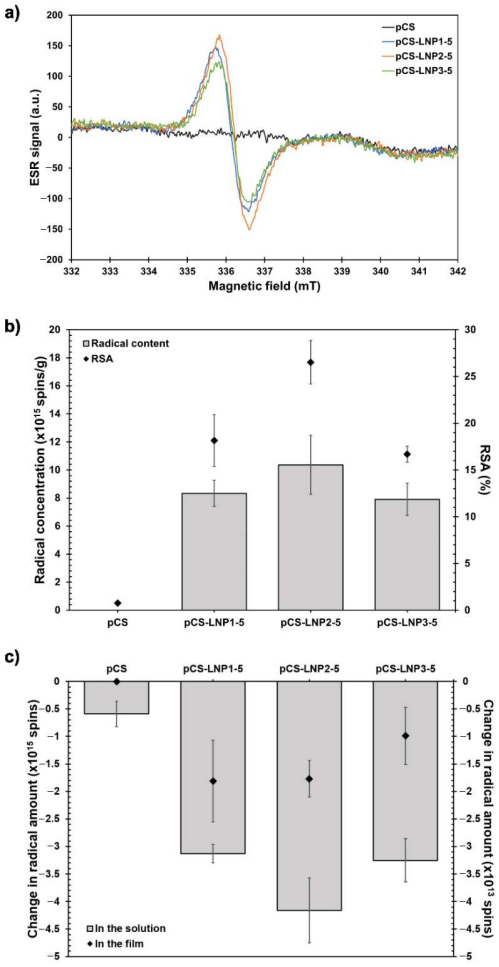

Figure 6. Radicals in films. (**a**) ESR spectra of pCS and pCS-LNP films. (**b**) Content of radicals in films and RSA of DPPH radicals in solutions measured after 30 min using ESR measurements. (**c**) Radical loss from film and from DPPH ethanol solution after 30 min contact with the film, both measured using ESR (**c**).

The stoichiometry of the changes in radical concentrations in the films and the surrounding DPPH solutions after 30 min contact were examined by calculating the losses of radicals (Figures 6c and S2). The amounts of radicals lost within the films after 30 min were similar for all the tested LNP-containing films, while two to three times higher amounts of DPPH had reacted in the surrounding solution outside the films (Figure 6c). The loss of the LNP radicals may be due to interaction with DPPH; however, it could also be due to the

increased mobility in the films in contact with the ethanol-water solvent as indicated by the migration and release of LNP fragments into the surrounding solutions.

4. Discussion: Perspectives on Film Properties and Antioxidant Activity

An overview of the film properties assessed in this study is given in Table 5. Summarizing the results, films with small LNPs had higher stiffness and tensile strength, good UV barrier properties and decent opacity properties. Only films containing LNP showed antioxidative properties, and films with medium-sized LNPs had a higher amount of migrating lignin-derived substances, higher initial content of radicals, and showed the highest antioxidant activity. The antioxidant effect is likely due to diffusion of lignin-derived phenolic substances out of the LNP-containing films. Although increasing LNP load improved UV barrier and antioxidant properties, it negatively affected opacity and mechanical properties, indicating that trade-offs and compromises might be necessary when developing these types of films for packaging applications.

Table 5. Effect of LNP size and loading on pCS-LNP films.

Property Comparison to pCS	Effect of LNP Loading			Effect of LNP Size at a Given Loading		
	1% (Low)	3% (Medium)	5% (High)	LNP1 (Small)	LNP2 (Medium)	LNP3 (Large)
Opacity	+	++	+++	++	+++	+++
UV barrier	+	++	+++	+++	+++	++
Young's modulus	+	+	+	+	0	0
Tensile strength	0	−	−−	0	−	−−
Elongation at break	−	−−	−−−	−−−	−−−	−−−
Antioxidant activity	+	++	+++	++	+++	+

"+" or "−" indicates an increase or a decrease; "0" indicates an insignificant effect.

Regarding the radical scavenging assay, ethanol was used to dissolve DPPH. Development of supplementary assays better suited for food types for which water is a more relevant solvent would be advantageous. If films both release antioxidants into the liquid and trap radicals at the film surface, observations will be a mixture of these two phenomena. For future studies of functional food packaging, an assay design that can capture such complex dynamics of antioxidant activity should be considered. Furthermore, the nature and rate of the migrating lignin-derived substances from LNPs, as well as the types of LNP-film biopolymer interactions, remain unknown and should be a subject of future studies. Clarifying these relationships is important as they can affect the actual antioxidant activity in specific applications and might potentially indirectly set the limits for other film properties because of the need to compromise.

5. Conclusions

Adding lignin nanoparticles to glycerol-plasticized chitosan film imparted higher UV-shielding properties to the resulting nanocomposite films but also made them stiffer, more brittle, and negatively affected opacity. These effects correlated with LNP loading. Smaller LNPs affected opacity less, and at the same time provided the best UV protection among the sizes tested, as well as resulting in stiffer and stronger films; i.e., they had a larger Young's modulus and higher tensile strength. Larger LNPs resulted in more uneven distribution of LNPs within the films and less smooth film surfaces.

The radical scavenging activity of the films correlated with the migration of phenolic lignin-derived substances out of the film. This was found to depend upon the size and distribution of the LNPs within the films, with films containing medium-sized LNPs

releasing most phenolics and having the highest antioxidant activity, showcasing the trade-off existing between the measured properties.

Supplementary Materials: The following supporting information can be downloaded at: https://www.mdpi.com/article/10.3390/suschem7010015/s1, Figure S1: Comparison of the opacity profiles (A/d, d is film thickness (mm)) for pCS, pCS-LNP1, pCS-LNP2, and pCS-LNP3 films at different LNP loading measured using UV-Vis spectrophotometry; Figure S2: Schematic of the experiment using ESR spectroscopy to measure RSA (%) and lost radical activity in the film and DPPH solution (spins), as well as a guide to where the corresponding results are shown in the main text; Table S1: Film thickness.

Author Contributions: Conceptualization, S.W. and D.T.D.; methodology, S.W., D.T.D., H.J.M., J.R. and M.L.A.; investigation, S.W., D.T.D., H.J.M., J.R. and M.L.A.; resources, L.G.T.; writing—original draft preparation, S.W. and D.T.D.; writing—review and editing, S.W., D.T.D., H.J.M., J.R., M.L.A. and L.G.T.; visualization, S.W.; supervision, L.G.T.; project administration, L.G.T.; funding acquisition, S.W., D.T.D. and L.G.T. All authors have read and agreed to the published version of the manuscript.

Funding: This research was supported by the Independent Research Fund Denmark (DFF, Odense, Denmark) [grant number 9041-00208B] and VILLUM FONDEN (Søborg, Denmark) [grant number 40950]. The APC was funded by The University of Copenhagen.

Data Availability Statement: The original contributions presented in this study are included in the article/supplementary material. Further inquiries can be directed to the corresponding author(s).

Acknowledgments: This research was supported by the Independent Research Fund Denmark (DFF, Odense, Denmark) [grant number 9041-00208B] and VILLUM FONDEN (Søborg, Denmark) [grant number 40950]. The Plant Nutrition group of Søren Husted at the Department of Plant and Environmental Sciences, University of Copenhagen is thanked for providing access to the Zetasizer instrument.

Conflicts of Interest: The authors declare that they have no known competing financial interests or personal relationships that could have appeared to influence the work reported in this paper.

Abbreviations

The following abbreviations are used in this manuscript:

CS	chitosan
DPPH	2,2-diphenyl-1-picrylhydrazyl
LNP	lignin nanoparticle
PBAT	poly(butylene adipate-co-terephthalate)
pCS	glycerol-plasticized chitosan films
PLA	(poly)lactic acid
PVA	polyvinyl alcohol
RSA	radical scavenging activity

References

1. Synowiecki, J.; Al-Khateeb, N.A. Production, Properties, and Some New Applications of Chitin and Its Derivatives. *Crit. Rev. Food Sci. Nutr.* **2003**, *43*, 145–171. [CrossRef] [PubMed]
2. Priyadarshi, R.; Rhim, J.W. Chitosan-Based Biodegradable Functional Films for Food Packaging Applications. *Innov. Food Sci. Emerg. Technol.* **2020**, *62*, 102346. [CrossRef]
3. Wang, H.; Qian, J.; Ding, F. Emerging Chitosan-Based Films for Food Packaging Applications. *J. Agric. Food Chem.* **2018**, *66*, 395–413. [CrossRef] [PubMed]
4. Nguyen, T.T.; Phan, N.-H.T.; Trinh, C.D.; Tran, T.V.; Pham, B.-T.T.; Quynh, B.T.P.; Phung, T.K. Glycerol-Plasticized Chitosan Film for the Preservation of Orange. *J. Food Saf.* **2022**, *42*, e12943. [CrossRef]
5. Ma, X.; Qiao, C.; Wang, X.; Yao, J.; Xu, J. Structural Characterization and Properties of Polyols Plasticized Chitosan Films. *Int. J. Biol. Macromol.* **2019**, *135*, 240–245. [CrossRef]

6. Rodríguez-Núñez, J.R.; Madera-Santana, T.J.; Sánchez-Machado, D.I.; López-Cervantes, J.; Soto Valdez, H. Chitosan/Hydrophilic Plasticizer-Based Films: Preparation, Physicochemical and Antimicrobial Properties. *J. Polym. Environ.* **2014**, *22*, 41–51. [CrossRef]
7. Thakhiew, W.; Devahastin, S.; Soponronnarit, S. Effects of Drying Methods and Plasticizer Concentration on Some Physical and Mechanical Properties of Edible Chitosan Films. *J. Food Eng.* **2010**, *99*, 216–224. [CrossRef]
8. Sun, Y.; Liu, Z.; Zhang, L.; Wang, X.; Li, L. Effects of Plasticizer Type and Concentration on Rheological, Physico-Mechanical and Structural Properties of Chitosan/Zein Film. *Int. J. Biol. Macromol.* **2020**, *143*, 334–340. [CrossRef]
9. Tripathi, S.; Mehrotra, G.K.; Dutta, P.K. Chitosan–Silver Oxide Nanocomposite Film: Preparation and Antimicrobial Activity. *Bull. Mater. Sci.* **2011**, *34*, 29–35. [CrossRef]
10. Priyadarshi, R.; Negi, Y.S. Effect of Varying Filler Concentration on Zinc Oxide Nanoparticle Embedded Chitosan Films as Potential Food Packaging Material. *J. Polym. Environ.* **2017**, *25*, 1087–1098. [CrossRef]
11. Rodrigues, C.; de Mello, J.M.M.; Dalcanton, F.; Macuvele, D.L.P.; Padoin, N.; Fiori, M.A.; Soares, C.; Riella, H.G. Mechanical, Thermal and Antimicrobial Properties of Chitosan-Based-Nanocomposite with Potential Applications for Food Packaging. *J. Polym. Environ.* **2020**, *28*, 1216–1236. [CrossRef]
12. Zhang, X.; Xiao, G.; Wang, Y.; Zhao, Y.; Su, H.; Tan, T. Preparation of Chitosan-Tio2 Composite Film with Efficient Antimicrobial Activities under Visible Light for Food Packaging Applications. *Carbohydr. Polym.* **2017**, *169*, 101–107. [CrossRef] [PubMed]
13. Sun, F.; Cha, H.R.; Bae, K.; Hong, S.; Kim, J.M.; Kim, S.H.; Lee, J.; Lee, D. Mechanical Properties of Multilayered Chitosan/Cnt Nanocomposite Films. *Mater. Sci. Eng. A* **2011**, *528*, 6636–6641. [CrossRef]
14. Swain, S.K.; Kisku, S.K.; Sahoo, G. Preparation of Thermal Resistant Gas Barrier Chitosan Nanobiocomposites. *Polym. Compos.* **2014**, *35*, 2324–2328. [CrossRef]
15. Chen, P.; Xie, F.W.; Tang, F.Z.; McNally, T. Influence of Plasticiser Type and Nanoclay on the Properties of Chitosan-Based Materials. *Eur. Polym. J.* **2021**, *144*, 110225. [CrossRef]
16. Casariego, A.; Souza, B.W.S.; Cerqueira, M.A.; Teixeira, J.A.; Cruz, L.; Díaz, R.; Vicente, A.A. Chitosan/Clay Films' Properties as Affected by Biopolymer and Clay Micro/Nanoparticles' Concentrations. *Food Hydrocoll.* **2009**, *23*, 1895–1902. [CrossRef]
17. Zhang, L.; Wang, H.; Jin, C.; Zhang, R.; Li, L.; Li, X.; Jiang, S. Sodium Lactate Loaded Chitosan-Polyvinyl Alcohol/Montmorillonite Composite Film Towards Active Food Packaging. *Innov. Food Sci. Emerg. Technol.* **2017**, *42*, 101–108. [CrossRef]
18. Alzagameem, A.; Bergrath, J.; Rumpf, J.; Schulze, M. Lignin-Based Composites for Packaging Applications. In *Micro and Nanolignin in Aqueous Dispersions and Polymers: Interactions, Properties, and Applications*; Elsevier: Amsterdam, The Netherlands, 2022; pp. 131–171. [CrossRef]
19. Luzi, F.; Torre, L.; Puglia, D. Polymeric Composites and Nanocomposites Containing Lignin: Structure and Applications. In *Micro and Nanolignin in Aqueous Dispersions and Polymers: Interactions, Properties, and Applications*; Elsevier: Amsterdam, The Netherlands, 2022; pp. 293–324. [CrossRef]
20. Schneider, W.D.H.; Dillon, A.J.P.; Camassola, M. Lignin Nanoparticles Enter the Scene: A Promising Versatile Green Tool for Multiple Applications. *Biotechnol. Adv.* **2021**, *47*, 107685. [CrossRef]
21. Tian, D.; Hu, J.; Bao, J.; Chandra, R.P.; Saddler, J.N.; Lu, C. Lignin Valorization: Lignin Nanoparticles as High-Value Bio-Additive for Multifunctional Nanocomposites. *Biotechnol. Biofuels* **2017**, *10*, 192. [CrossRef]
22. Yang, W.; Owczarek, J.S.; Fortunati, E.; Kozanecki, M.; Mazzaglia, A.; Balestra, G.M.; Kenny, J.M.; Torre, L.; Puglia, D. Antioxidant and Antibacterial Lignin Nanoparticles in Polyvinyl Alcohol/Chitosan Films for Active Packaging. *Ind. Crops Prod.* **2016**, *94*, 800–811. [CrossRef]
23. Yang, W.; Qi, G.; Kenny, J.M.; Puglia, D.; Ma, P. Effect of Cellulose Nanocrystals and Lignin Nanoparticles on Mechanical, Antioxidant and Water Vapour Barrier Properties of Glutaraldehyde Crosslinked Pva Films. *Polymers* **2020**, *12*, 1364. [CrossRef] [PubMed]
24. Yang, W.; Qi, G.; Ding, H.; Xu, P.; Dong, W.; Zhu, X.; Zheng, T.; Ma, P. Biodegradable Poly (Lactic Acid)-Poly (E-Caprolactone)-Nanolignin Composite Films with Excellent Flexibility and Uv Barrier Performance. *Compos. Commun.* **2020**, *22*, 100497. [CrossRef]
25. Yang, W.; Fortunati, E.; Dominici, F.; Giovanale, G.; Mazzaglia, A.; Balestra, G.M.; Kenny, J.M.; Puglia, D. Synergic Effect of Cellulose and Lignin Nanostructures in Pla Based Systems for Food Antibacterial Packaging. *Eur. Polym. J.* **2016**, *79*, 1–12. [CrossRef]
26. Xing, Q.; Buono, P.; Ruch, D.; Dubois, P.; Wu, L.; Wang, W.-J. Biodegradable Uv-Blocking Films through Core–Shell Lignin–Melanin Nanoparticles in Poly(Butylene Adipate-Co-Terephthalate). *ACS Sustain. Chem. Eng.* **2019**, *7*, 4147–4157. [CrossRef]
27. Vijayakumar, R.; Sivaraman, Y.; Pavagada Siddappa, K.M.; Dandu, J.P.R. Synthesis of Lignin Nanoparticles Employing Acid Precipitation Method and Its Application to Enhance the Mechanical, Uv-Barrier and Antioxidant Properties of Chitosan Films. *Int. J. Polym. Anal. Charact.* **2022**, *27*, 99–110. [CrossRef]
28. Zhang, W.; Gao, P.; Jiang, Q.; Xia, W. Green Fabrication of Lignin Nanoparticles/Chitosan Films for Refrigerated Fish Preservation Application. *Food Hydrocoll.* **2023**, *139*, 108548. [CrossRef]

29. Zhang, Z.; Argenziano, R.; Konate, A.; Shi, X.; Salazar, S.A.; Cerruti, P.; Panzella, L.; Terrasson, V.; Guénin, E. Preparation of Chitosan/Lignin Nanoparticles-Based Nanocomposite Films with High-Performance and Improved Physicochemical Properties for Food Packaging Applications. *Int. J. Biol. Macromol.* **2025**, *293*, 139079. [CrossRef]
30. Ashraf, M.A.; Peng, W.; Zare, Y.; Rhee, K.Y. Effects of Size and Aggregation/Agglomeration of Nanoparticles on the Interfacial/Interphase Properties and Tensile Strength of Polymer Nanocomposites. *Nanoscale Res. Lett.* **2018**, *13*, 214. [CrossRef]
31. Kontou, E.; Christopoulos, A.; Koralli, P.; Mouzakis, D.E. The Effect of Silica Particle Size on the Mechanical Enhancement of Polymer Nanocomposites. *Nanomaterials* **2023**, *13*, 1095. [CrossRef]
32. Fu, S.Y.; Feng, X.Q.; Lauke, B.; Mai, Y.W. Effects of Particle Size, Particle/Matrix Interface Adhesion and Particle Loading on Mechanical Properties of Particulate-Polymer Composites. *Compos. Part B Eng.* **2008**, *39*, 933–961. [CrossRef]
33. Gómez-Estaca, J.; López-de-Dicastillo, C.; Hernández-Muñoz, P.; Catalá, R.; Gavara, R. Advances in Antioxidant Active Food Packaging. *Trends Food Sci. Technol.* **2014**, *35*, 42–51. [CrossRef]
34. Cheng, H.; Chen, L.; McClements, D.J.; Xu, H.; Long, J.; Zhao, J.; Xu, Z.; Meng, M.; Jin, Z. Recent Advances in the Application of Nanotechnology to Create Antioxidant Active Food Packaging Materials. *Crit. Rev. Food Sci. Nutr.* **2022**, *64*, 2890–2905. [CrossRef]
35. Sadeghifar, H.; Ragauskas, A.J. Lignin as a Natural Antioxidant: Chemistry and Applications. *Macromol* **2025**, *5*, 5. [CrossRef]
36. Benbettaïeb, N.; Mahfoudh, R.; Moundanga, S.; Brachais, C.-H.; Chambin, O.; Debeaufort, F. Modeling of the Release Kinetics of Phenolic Acids Embedded in Gelatin/Chitosan Bioactive-Packaging Films: Influence of Both Water Activity and Viscosity of the Food Simulant on the Film Structure and Antioxidant Activity. *Int. J. Biol. Macromol.* **2020**, *160*, 780–794. [CrossRef] [PubMed]
37. Crouvisier-Urion, K.; Bodart, P.R.; Winckler, P.; Raya, J.; Gougeon, R.D.; Cayot, P.; Domenek, S.; Debeaufort, F.; Karbowiak, T. Biobased Composite Films from Chitosan and Lignin: Antioxidant Activity Related to Structure and Moisture. *ACS Sustain. Chem. Eng.* **2016**, *4*, 6371–6381. [CrossRef]
38. Sipponen, M.H.; Lange, H.; Ago, M.; Crestini, C. Understanding Lignin Aggregation Processes. A Case Study: Budesonide Entrapment and Stimuli Controlled Release from Lignin Nanoparticles. *ACS Sustain. Chem. Eng.* **2018**, *6*, 9342–9351. [CrossRef] [PubMed]
39. Zou, T.; Sipponen, M.H.; Österberg, M. Natural Shape-Retaining Microcapsules with Shells Made of Chitosan-Coated Colloidal Lignin Particles. *Front. Chem.* **2019**, *7*, 370.
40. Riaz, A.; Lei, S.; Akhtar, H.M.S.; Wan, P.; Chen, D.; Jabbar, S.; Abid, M.; Hashim, M.M.; Zeng, X. Preparation and Characterization of Chitosan-Based Antimicrobial Active Food Packaging Film Incorporated with Apple Peel Polyphenols. *Int. J. Biol. Macromol.* **2018**, *114*, 547–555. [CrossRef]
41. Sadeer, N.B.; Montesano, D.; Albrizio, S.; Zengin, G.; Mahomoodally, M.F. The Versatility of Antioxidant Assays in Food Science and Safety-Chemistry, Applications, Strengths, and Limitations. *Antioxidants* **2020**, *9*, 709. [CrossRef]
42. Rambabu, K.; Bharath, G.; Banat, F.; Show, P.L.; Cocoletzi, H.H. Mango Leaf Extract Incorporated Chitosan Antioxidant Film for Active Food Packaging. *Int. J. Biol. Macromol.* **2019**, *126*, 1234–1243. [CrossRef]
43. Abdollahi, M.; Rezaei, M.; Farzi, G. Improvement of Active Chitosan Film Properties with Rosemary Essential Oil for Food Packaging. *Int. J. Food Sci. Tech.* **2012**, *47*, 847–853. [CrossRef]
44. Galus, S.; Arik Kibar, E.A.; Gniewosz, M.; Kraśniewska, K. Novel Materials in the Preparation of Edible Films and Coatings—A Review. *Coatings* **2020**, *10*, 674. [CrossRef]
45. Yen, M.T.; Yang, J.H.; Mau, J.L. Antioxidant Properties of Chitosan from Crab Shells. *Carbohydr. Polym.* **2008**, *74*, 840–844. [CrossRef]
46. Kuai, L.; Liu, F.; Chiou, B.-S.; Avena-Bustillos, R.J.; McHugh, T.H.; Zhong, F. Controlled Release of Antioxidants from Active Food Packaging: A Review. *Food Hydrocoll.* **2021**, *120*, 106992. [CrossRef]
47. Bährle, C.; Nick, T.U.; Bennati, M.; Jeschke, G.; Vogel, F. High-Field Electron Paramagnetic Resonance and Density Functional Theory Study of Stable Organic Radicals in Lignin: Influence of the Extraction Process, Botanical Origin, and Protonation Reactions on the Radical G Tensor. *J. Phys. Chem. A* **2015**, *119*, 6475–6482. [CrossRef]